SAND2017-2521J

Geophysical Research Letters

Supporting Information for

Drought Conditions Maximize the Impact of High-Frequency Flow Variations on Thermal Regimes and Biogeochemical Function in the Hyporheic Zone

Xuehang Song[1], Xingyuan Chen[1,*], James Stegen[1], Glenn Hammond[2], Heng Dai[1], Emily Graham[1], and John M. Zachara[1]

[1]Pacific Northwest National Laboratory, Richland, Washington, USA.

[2]Applied Systems Analysis and Research, Sandia National Laboratories, Albuquerque, New Mexico, USA.

Contents of this file

Introduction

This supplementary information contains: 1) methodology of the wavelet spectral analysis; 2) hydraulic and thermal parameters in the model setup; 3) more details about the cybernetic model; and 4) additional simulation results, e.g., temperature results of the case with daily smoothed boundary, carbon consumption distribution of individual reactions, and analyses of individual reactions.

Text S1.

Methodology of the wavelet spectral analysis

We conducted the wavelet spectral analysis using the R package "WaveletComp" [*Roesch and Schmidbauer*, 2015], where the Morlet "mother" wavelet was defined as:

$$\psi_0(t) = \pi^{-1/4} e^{i\omega t} e^{-t^2/2}, \tag{S1}$$

where the dimensionless frequency ω is set as 6 and *t* is time. The continuous wavelet transform of a time series is defined as the convolution of the series with a set of "daughter" wavelets as:

$$\mathrm{Wave}(\tau, s) = \sum_t x_t \frac{1}{\sqrt{s}} \psi_0^* \left(\frac{t-\tau}{s} \right), \tag{S2}$$

where x_t is the time series to be decomposed and * denotes the complex conjugate. The localizing time parameter τ and a time increment dt are used to determine the daughter wavelet's location in the time domain. In this study, the dt is defined as the minimal observation interval. The scaling parameter *s* determines the daughter wavelet's coverage in the frequency domain. The wavelet power spectrum describes the time frequency (or time period) wavelet energy density as:

$$\mathrm{Power}(\tau, s) = \frac{1}{s} \left| \mathrm{Wave}(\tau, s) \right|^2. \tag{S3}$$

The time-averaged wavelet power spectrum for each scale parameter s is then calculated to measure the significance of certain frequencies (periods) in the evaluated time series.

Text S2.

Hydraulic and thermal properties

The hydraulic and thermal properties were taken and modified from studies in the same site [*Ma et al.*, 2012; *Chen et al.*, 2013], as show in Table S2.

Text S3.

Mass balance equations of the cybernetic model

For the compact form (vector-matrix representation) of the reaction equation Eq. (3) in the main text, we can derive:

$$\frac{d}{dt}\begin{bmatrix}[DOC]\\ [O_2]\\ [NO_3^-]\\ [NO_2^-]\\ [N_2]\\ [CO_2]\\ [BM]\end{bmatrix}=\begin{bmatrix}-1 & -1 & -1\\ 0 & 0 & -f_3\\ -2f_1 & 0 & 0\\ 2f_1 & -4f_2/3 & 0\\ 0 & 3f_2/2 & 0\\ f_1 & f_2 & f_3\\ (1-f_1)/5 & (1-f_2)/5 & (1-f_3)/5\end{bmatrix}\begin{bmatrix}r_1\\ r_2\\ r_3\end{bmatrix}[BM], \quad \text{(S4)}$$

where r_1, r_2, and r_3 are the regulated reactions rates for aerobic respiration and denitrification.

We further modified the preceding partial differential equation by accounting the biomass degradation ratio K_{deg}. For the dissolved organic carbon (DOC) and biomass balance, we can derive:

$$\frac{d[DOC]}{dt}=-\left(r_1+r_2+r_3-5k_{\deg}\right)[BM] \quad \text{(S5)}$$

$$\frac{d[BM]}{dt}=\left(\frac{1-f_1}{5}r_1+\frac{1-f_2}{5}r_2+\frac{1-f_3}{5}r_3-k_{\deg}\right)[BM] \quad \text{(S6)}$$

These reaction equations were coded in PFLOTRAN's reaction sandbox.

Reaction parameters and model fitting of batch experimental data

The reaction parameters for the cybernetic model are listed in Table S3.1. The model fit for laboratory batch denitrification data is shown in Figure S3. The solute concentrations of inland/river boundaries are listed in Table S3.2.

Text S4.

This section provides more model results with additional details that did not result in any new or change the conclusions in the main text.

Temperature results of case with daily smoothed hydraulic boundaries

In the main text, only the baseline case temperature and its difference between the weekly smoothed case were presented in Figure 3. As such, we put the results of the daily smoothed case in Figure S4.1 as a supplement. The difference between the base and daily smoothed cases was reasonably smaller than the difference between the base and weekly smoothed cases. All conclusions based on the weekly smoothed case stated in the main text hold for the daily case.

Cumulative carbon consumption distribution of individual reaction

In the main text, only the total cumulative carbon consumption distribution was shown in Figure 4. We did not include the cumulative carbon consumption distribution of individual reactions as they all had similar patterns, and most carbon was consumed in oxidative respiration (Figure S4.2).

Carbon consumption rates comparison

In the main text, only the total carbon consumption rates were compared between the base and weekly smoothed cases. In Figure S4, we included such a comparison across different reactions and cases as a supplement. The same conclusions can be derived as presented in the main text.

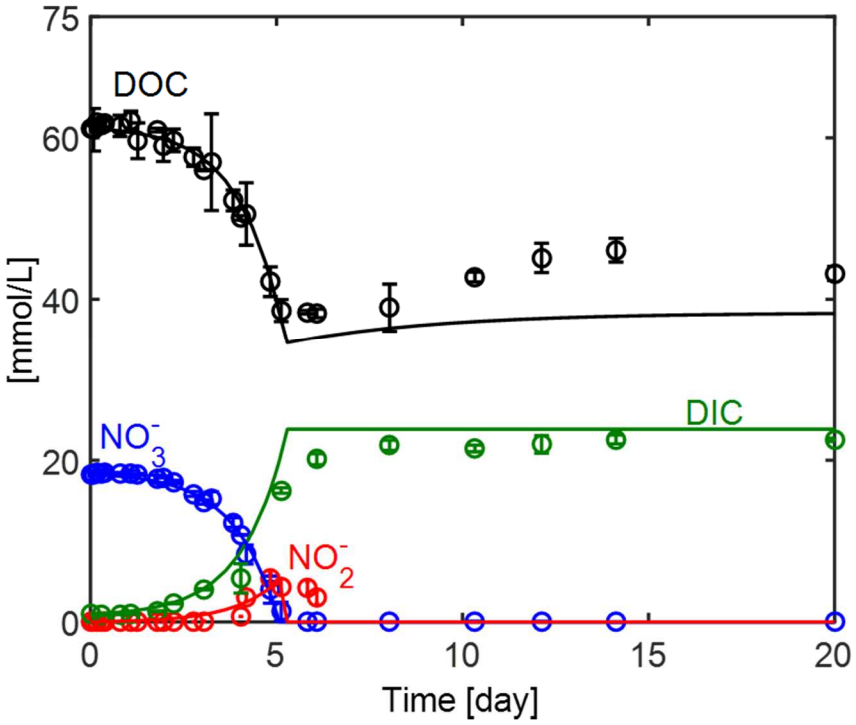

Figure S3. Model fit to batch denitrification data

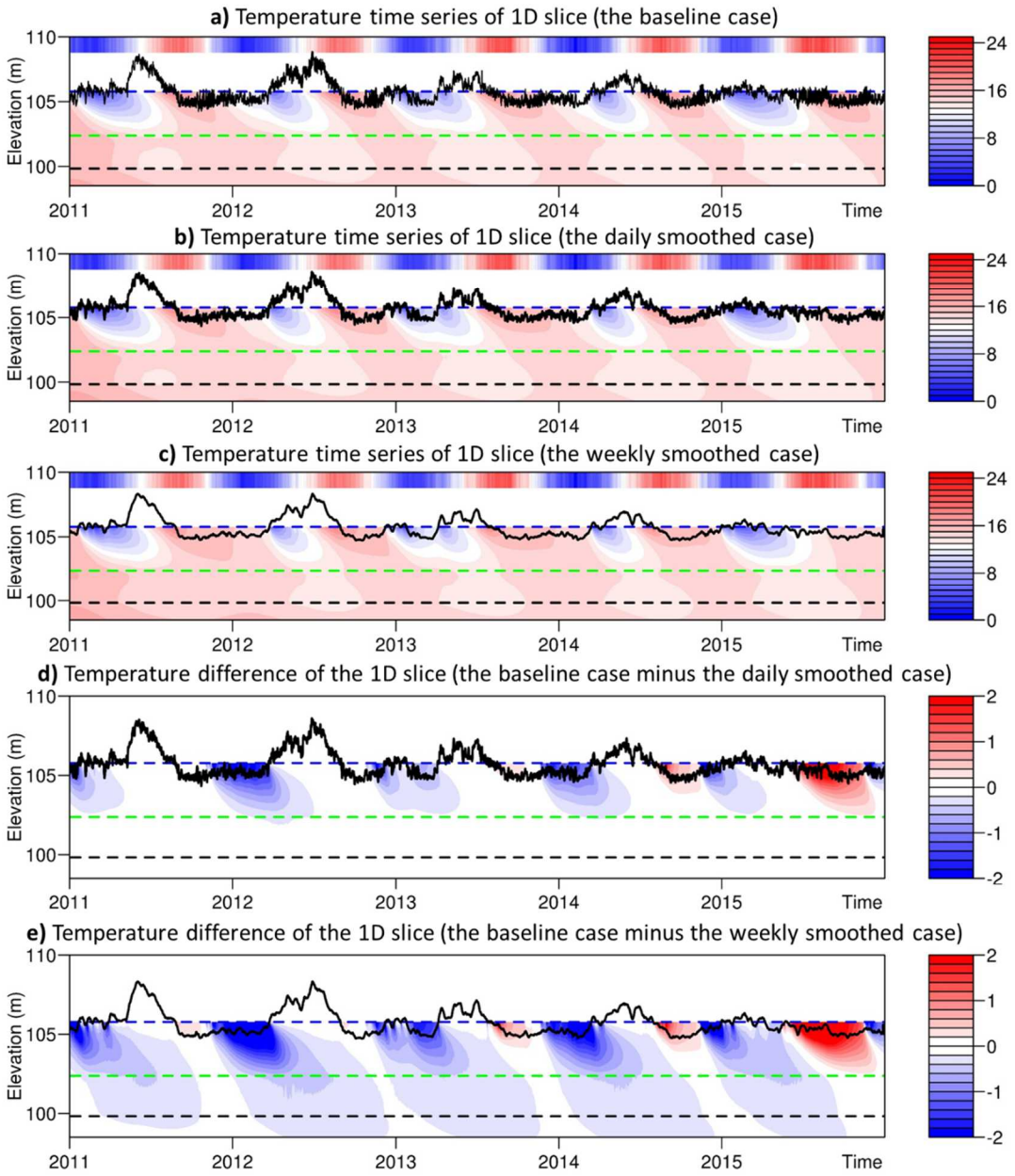

Figure S4.1. Temperature simulation results: a) Temperature time series of a 1D slice (the vertical line in the Figure 3a in the main text) of the baseline case to illustrate the temperature lags in the HZ. The top crossband shows the temperature of river water. The black curve is the river stage, the colored dash lines are the formation boundaries, and the bottom part is the temperature dynamics in this column; b) Temperature time series of the 1D slice of the daily smoothed case; c) Temperature time series of the 1D slice of the weekly smoothed case; d) Temperature difference of the 1D slice (the baseline case minus the daily smoothed case); e) Temperature difference of the 1D slice (the baseline case minus the weekly smoothed case). The a) and e) are featured in the main text (Figure 4) and placed here only for comparison.

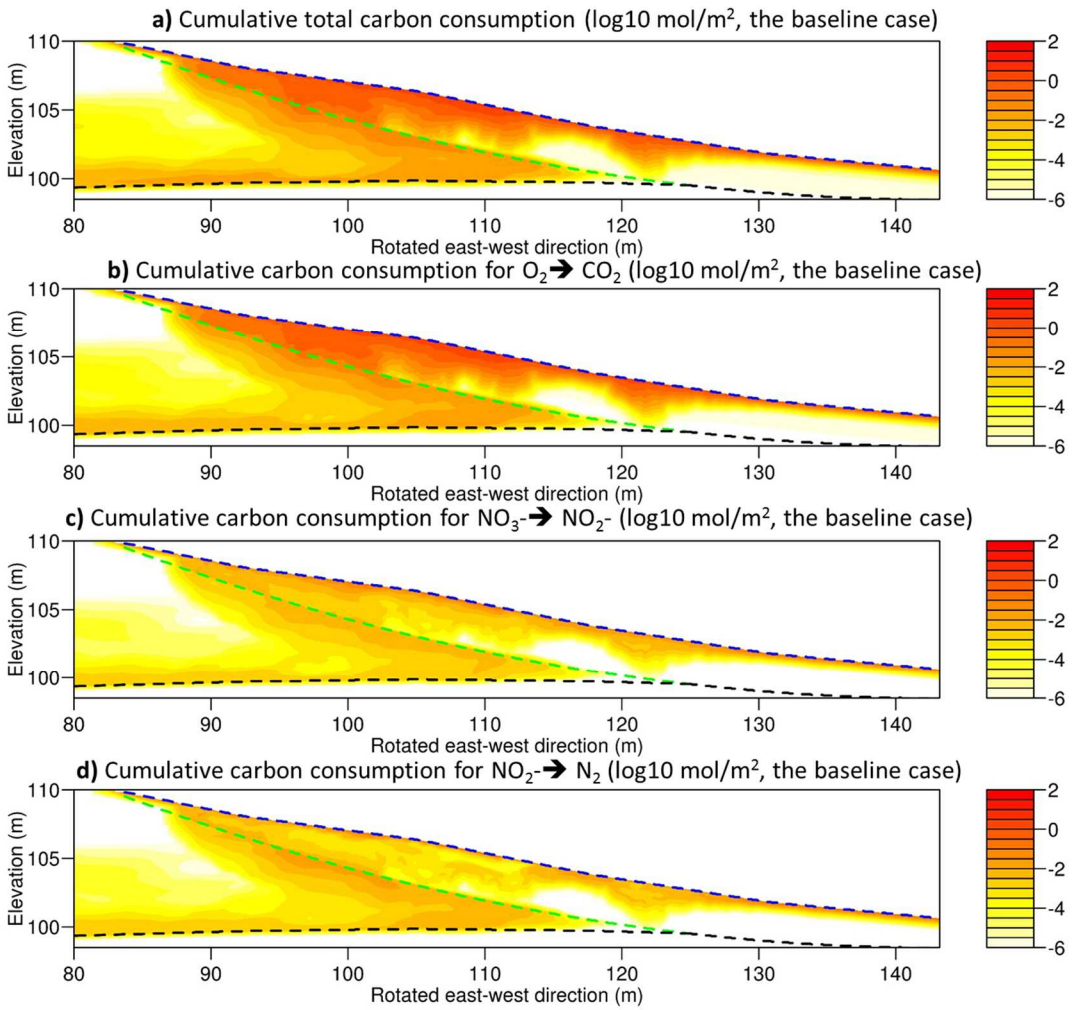

Figure S4.2. Cumulative carbon consumption for individual reactions (log10, mol/m^2): a) Total carbon consumption; b) O_2➔CO_2; c) NO_3^- ➔NO_2^-; d) NO_3➔N_2. Image a) was included in the main text (Figure 4) and placed here again only for comparison.

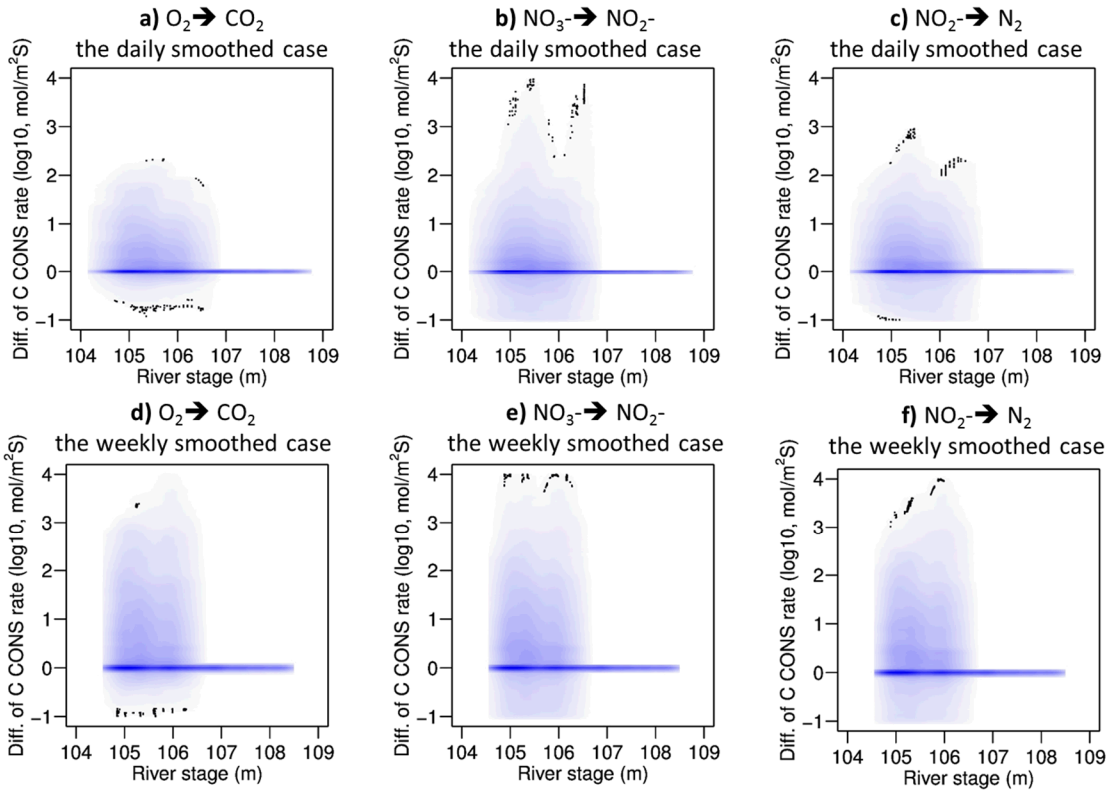

Figure S4.3. River stage versus carbon consumption rate difference between the baseline case and other cases in entire alluvium: a) O_2➔CO_2 (the baseline case minus the daily smoothed case); b) NO_3^-➔NO_2^- (the baseline case minus the daily smoothed case); c) NO_2➔N_2 (the baseline case minus the daily smoothed case); d) O_2➔CO_2 (the baseline case minus the weekly smoothed case); e) NO_3^- ➔NO_2^- (the baseline case minus the weekly smoothed case); f) NO_2➔N_2 (the baseline case minus the weekly smoothed case).

	Hanford	alluvium	Ringold
Geostatistical parameters of permeability field (exponential variogram)			
Mean (log, m^2)	-8.13	-13	-15
SD (log, m^2)	0.83	0.81	homogenous
Integral scale (m)	20	8	homogenous
Anisotropy ratio	0.1	0.1	homogenous
Anisotropy angle (◦)	-3	9	homogenous
Nugget	0	0	homogenous
Other hydraulic properties			
Porosity (-)	0.2	0.43	0.43
Residual saturation (-)	0.16	0.13	0.13
van Genuchten alpha parameter (Pa^{-1})	7.27e-4	1.43e-4	1.43e-4
van Genuchten m parameter [-]	0.34	0.75	0.75
Thermal properties			
Soil particle density of material (kg/m^3)	2760	2650	2650
Specific heat capacity of material (J/kg·K)	715	920	920
Wet thermal conductivity of material (W/K·m)	1.88	0.93	0.93
Dry thermal conductivity of material (W/K·m)	0.93	0.68	0.68

Table S2. Hydraulic and thermal properties of Hanford/alluvium/Ringold in the 2D model

Parameter	NO_3^-➔NO_2^-	NO_2^-➔N_2	O_2➔CO_2	Source
f_i [-]	$f_1 = 0.65$	$f_2 = 0.99$	Estimated as $f_3 = 1/3\ f_1$	Data fit
K_i [mmol/mmol BM/d]	$K_1 = 28.26$	$K_2 = 23.28$	$K_3 = 3\ K_1$ [*Gu et al.*, 2012]	Data fit
$K_{d,i}$[mM]	$K_{d,1} = 0.25$	$K_{d,2} = 0.25$	Estimated as $K_{d,3} = K_{d,1}$	[*Yan et al*., 2016]
$K_{a,i}$[mM]	$K_{a,1} = 0.001$	$K_{a,2} = 0.004$	Estimated as $K_{a,3} = K_{a,1}$	[*Rittmann*, 2001]
k_{deg} [mmol/mmol BM/d]	0.242		Data fit	

Table S3.1. Biogeochemical reaction parameters

Solute	Inland	River
CH_2O [mol/L]	4.16e-5	2.58e-4
CO_2 [mol/L]	2.48e-3	1.12e-3
NO_3- [mol/L]	3.96e-4	8.87e-6
O_2 [mol/L]	2.67e-4	3.59e-4
$C_5H_7O_2N$ [mol/L]	1.00e-5	1.00e-5
N_2 [mol/L]	1e-10	1e-10
NH_{4+} [mol/L]	1e-10	1e-10
NO_2- [mol/L]	1e-10	1e-10

Table S3.2. Solute concentration on boundaries (N_2, NH_{4+}, and NO_2- is minimum)

Drought Conditions Maximize the Impact of High-Frequency Flow Variations on Thermal Regimes and Biogeochemical Function in the Hyporheic Zone

Xuehang Song[1], Xingyuan Chen[1, *], James Stegen[1], Glenn Hammond[2], Heng Dai[1], Emily Graham[1], and John M. Zachara[1]

[1]Pacific Northwest National Laboratory, Richland, Washington, USA.

[2]Applied Systems Analysis and Research, Sandia National Laboratories, Albuquerque, New Mexico, USA.

*Corresponding author

Email: Xingyuan.Chen@pnnl.gov; Phone: (509) 371-7510; Fax: (509) 375-2999

Key Points

- High-frequency flow variations enhance hyporheic exchange, increase biogeochemical fluxes, and create long-term alterations to thermal regimes.
- The spatial distribution of biogeochemical hot spots depends highly on the subsurface hydraulic properties instead of high-frequency flow variations.
- The high-frequency flow variations under drought conditions lead to warmer hyporheic temperatures that could potentially affect riverine ecosystems.

Abstract

Anthropogenic activities, such as dam operations, often induce larger and more frequent stage fluctuations than those occurring in natural rivers. However, the long-term impact of such flow variations on thermal and biogeochemical dynamics of the associated hyporheic zone (HZ) is poorly understood. A heterogeneous, two-dimensional thermo-hydro-biogeochemical model revealed an important interaction between high-frequency flow variations and watershed-scale hydrology. High-frequency stage fluctuations had their strongest thermal and biogeochemical impacts when the mean river stage was low during fall and winter. An abnormally thin snowpack in 2015, however, created a low river stage during summer and early fall, whereby high-frequency stage fluctuations caused the HZ to be warmer than usual. This study provided the scientific basis to assess the potential ecological consequences of the high-frequency flow variations in a regulated river, as well as guidance on how to maximize the potential benefits—or minimize the drawbacks—of river regulation to river ecosystems.

1. Introduction

The hyporheic zone (HZ) is a transition area where groundwater mixes with surface water and mediates the surface-subsurface exchange of water, heat, and solutes (e.g., dissolved oxygen, organic carbon, carbon dioxide, nitrate, and ammonium) [*Boano et al.*, 2014; *Brunke and Gonser*, 1997]. Surface-subsurface flow interactions in the HZ are critical in aquatic environments, where biogeochemical processes often are enhanced because of waters mixing from different sources [*McClain et al.*, 2003; *Battin et al.*, 2008; *Cardenas*, 2015; *Stegen et al.*, 2016]. Multiple complex physical features influence the extent of the HZ and additional bank storage [*Boulton et al.*, 1998]. These include sediment permeability and porosity [*Cardenas et al.*, 2004; *Salehin et al.*, 2004]; river morphology, such as riffle, bars, and dunes [*Cardenas and Wilson*, 2007;

61 *Buffington and Tonina*, 2009; *Stonedahl et al.*, 2013]; and dynamic hydrologic boundary
62 conditions [S*chmadel et al.*, 2016].

63

64 The dynamic hydrologic boundary condition of the HZ exchange is controlled not only by
65 natural processes (e.g., snowmelt, precipitation, flood, and tidal cycles) but also by
66 anthropogenic activity, such as dam operations. In the United States [*Graf*, 1999] and across the
67 globe [*Nilsson et al.*, 2005], dam construction in large river systems has been widespread. Rivers
68 regulated by dams often experience large and dynamic stage fluctuations to meet the combined
69 demands of hydropower, irrigation, and flood control. Frequent river stage fluctuations can
70 significantly alter the hydraulic gradient between groundwater and surface water [*Arntzen et al.*,
71 2006; *Fritz and Arntzen*, 2007], with consequent changes to the thermal [*Sawyer et al.*, 2009;
72 *Slater et al.*, 2010*; Gerecht et al.*, 2011] and biogeochemical dynamics [*Ye et al.*, 2012; *Gu et al.*,
73 2012; *Briody et al.*, 2016; *Trauth and Fleckenstein,* 2017] in the HZ by creating more frequent
74 changes in gaining/losing conditions for streams or aquifers compared to steady state flow
75 conditions [*Sawyer et al.*, 2009; *Francis et al.*, 2010; *Gerecht et al.*, 2011; *Graham et al.*, 2015;
76 *Yellen and Boutt*, 2015]. Both the thermal and biogeochemical processes in the HZ play
77 important roles in fluvial ecology, such as benthic food production, salmonid growth [*Mejia et*
78 *al.*, 2016], and fish spawning [*Hanrahan*, 2007; *Casas-Mulet et al.*, 2016]. The temperature of
79 upwelling HZ water is especially important to temperature-sensitive organisms [*Geist et al.*,
80 2002; *Ebersole et al.*, 2003; *Galbraith et al.*, 2012; *Mejia et al.*, 2016].

81

82 The conceptual representation of heat transport and biogeochemical processes in the HZ of a
83 regulated river often has been ignored or over-simplified by neglecting dynamic river stage
84 fluctuations. Furthermore, most studies have investigated only the short-term (days to weeks)
85 impacts of dynamic river stage fluctuations on the hyporheic temperature and biogeochemical
86 functions, while longer-term (seasonal to interannual) impacts could result from the potentially
87 long residence time of intruded river water in the associated groundwater system. For example,
88 the heat storage effect of the HZ can persist for months [*Arrigoni et al.*, 2008; *Burkholder et al.*,
89 2008], and the riverbed redox conditions can be impacted by seasonal hydrograph cycles [*Lautz*
90 *and Fanelli*, 2008]. Addressing the long-term effects of flow variations on hyporheic thermal and
91 biogeochemical processes requires extended observational and modeling studies with a realistic
92 representation of heat transport, biogeochemical processes, and water exchange fluxes.

93

94 In this letter, we address the following question: how do high-frequency flow variations, driven
95 mainly by dam operations to meet hydropower demands, control temperature dynamics and
96 biogeochemical fluxes in the HZ? Such understanding could provide the scientific basis needed
97 to assess the potential ecological consequences of high-frequency flow variations caused by
98 anthropogenic perturbations. To address these impacts and linkages, we applied a fully coupled,
99 two-dimensional (2D) thermo-hydro-biogeochemical model with realistically heterogeneous
100 sediment properties along a transect perpendicular to the Columbia River. The hydrologic
101 boundary conditions (e.g., river stage and groundwater table) were progressively smoothed to
102 remove high-frequency fluctuations. Multi-year simulations were conducted using the field-
103 observed and smoothed hydrologic boundary conditions. The differences in their respective
104 results of temperature dynamics, velocity, and cumulative carbon/consumption in the HZ were

105 used to assess the impacts of high-frequency flow variations. We found that high-frequency (sub-
106 daily to weekly) flow variations had a larger impact on the HZ thermal regimes and
107 biogeochemical function when the river stage was low, whereas zones with enhanced
108 biogeochemical activity and associated fluxes were strongly dependent on the physical
109 heterogeneity of the riverbed's alluvial layer.

110 **2. Methodology**

111 **2.1 Site Description**

112 The study area is situated on the Hanford Reach's western shore on the Columbia River in the
113 300 Area of the U.S. Department of Energy's Hanford Site (Figure 1a), located within the
114 semiarid Pasco Basin in southeastern Washington State. The Hanford Reach is an 80 km free-
115 flowing section of the Columbia River with hydroelectric dams at its upstream (Priest Rapids)
116 and downstream (McNary) boundaries [*Duncan et al.*, 2007]. The unconfined aquifer that exists
117 within the river corridor and extends beneath the riverbed can be delineated into three distinct
118 geologic formations: low-permeability sandy alluvium, highly permeable Hanford gravels, and
119 low-permeability Ringold fluvial deposits [*Williams et al.*, 2008].

120 **2.2 Spectral Decomposition of Dam Discharge and River Stage**

121 The river stage observed at our study site fluctuates ~0.5 meters daily and up to 2-3 meters
122 annually. The high-frequency variations (sub-daily to weekly) in river stage are driven by dam
123 operations upstream from the study site. A wavelet-based spectral analysis method (refer to
124 Supporting Information) was applied to determine dominant frequencies of variations in the time
125 series of: 1) the observed river stage and 2) observed (dam-impacted) and naturalized (assuming
126 no dam operation or irrigation) discharges below the Priest Rapids Dam. The discharge data
127 were obtained from the River Management Joint Operating Committee (RMJOC)

128 (http://www.bpa.gov/power/streamflow/default.aspx). The frequencies of variations caused by
129 the upstream dam operation were identified by cross-comparing dominant frequencies in the
130 spectral analysis results. The moving average then was applied as a low-pass filter to remove
131 those high frequencies in the river stage and inland groundwater table. The smoothed/filtered
132 hydrologic boundary conditions were used to drive model simulations without impacts of high-
133 frequency flow variations and compared with the simulation under unfiltered highly dynamic
134 hydrologic boundary conditions. The difference between simulated hyporheic exchange and
135 associated biogeochemical processes represents the effects of dam-induced high-frequency flow
136 variations on hyporheic processes.
137
138 **2.3 Numerical Model Configuration**
139 To simulate lateral and vertical HZ exchange, we constructed a 2D model with the river and
140 inland aquifer as two end members of the river corridor system. The 2D model's geological
141 structure was informed by previous geological and geophysical surveys [*Williams et al.*, 2008;
142 *Chen et al.*, 2013]. Heterogeneous permeability fields of the alluvium and Hanford gravels
143 (Figure 1b) were generated with unconditional geostatistical simulations using the R package
144 "gstat" [*Pebesma*, 2004] to investigate the potential impact of preferential flow in the alluvium
145 and Hanford gravel. The hydraulic and thermal properties were modified from earlier modeling
146 studies performed at the same site [*Ma et al*., 2012; *Chen et al*., 2013] (more information is
147 provided in the Supporting Information). The model domain was 143.2 m in the horizontal
148 direction and 20 m in the vertical. The grid size was refined near the shoreline (a rectangle
149 covering the entire alluvium and its surrounding Hanford and Ringold formation sediments) with
150 cells measured at 0.1 m in the horizontal and 0.05 m in the vertical to capture the HZ's detailed

151 exchange dynamics. To avoid numerical instability, the grid sizes for the rest of the domain were
152 progressively increased by 9%. The total number of grid cells was nearly 0.2 million.

153 **2.3.1 Biogeochemical Functions**

154 Oxidative respiration and two-step denitrification were considered representative HZ
155 biogeochemical processes in the simulated reaction network:

$$\begin{aligned} &CH_2O + O_2 \rightarrow CO_2 + H_2O \\ &CH_2O + 2NO_3^- \rightarrow 2NO_2^- + CO_2 + H_2O \\ &CH_2O + 4/3NO_2^- + 4/3H^+ \rightarrow 2/3N_2 + CO_2 + 5/3H_2O \end{aligned} \quad . \tag{1}$$

157 Microbial biomass ($1/5C_5H_7O_2N$) synthesis was considered as:

$$CH_2O + 1/5NH_4^+ \rightarrow 1/5C_5H_7O_2N + 3/5H_2O + 1/5H^+ . \tag{2}$$

159 Oxidative respiration and denitrification were combined with biomass synthesis according to the
160 following relationships:

$$\begin{aligned} &CH_2O + 2f_1NO_3^- + \frac{1}{5}(1-f_1)NH_4^+ \rightarrow 2f_1NO_2^- + f_1CO_2 + \frac{1}{5}(1-f_1)C_5H_7O_2N \\ &CH_2O + 2f_2NO_2^- + \frac{1}{5}(1-f_2)NH_4^+ \rightarrow \frac{2}{3}f_2N_2 + f_2CO_2 + \frac{1}{5}(1-f_2)C_5H_7O_2N \\ &CH_2O + f_3O_2 + \frac{1}{5}(1-f_3)NH_4^+ \rightarrow f_3CO_2 + \frac{1}{5}(1-f_3)C_5H_7O_2N \end{aligned} \quad , \tag{3}$$

162 where f_1, f_2, and f_3 denote the energy-producing fraction parameters.

163 Reaction rates for the oxidative respiration and two-step denitrification in Eq. (3) were modeled
164 as being catalyzed by specific enzymes:

$$r_i = e_i r_i^{kin} , \tag{4}$$

166 where i is the generic reaction index, e_i is the relative level of enzymes (described later), and r_i^{kin}
167 is the unregulated reaction rate (mol $L^{-1}d^{-1}$) represented using double Monod kinetics:

$$r_i^{kin} = k_i \frac{d_i}{K_{d,i} + d_i} \frac{a_i}{K_{a,i} + a_i} \quad . \tag{5}$$

Here, k_i is the maximum specific uptake rate of microbial reaction (mol $L^{-1}d^{-1}$), a_i is the electron acceptor concentration (mol L^{-1}), $K_{a,i}$ is the half-saturation constant for electron acceptors, d_i (mol L^{-1}) is the electron acceptor concentration (mol L^{-1}), and $K_{d,i}$ is the half-saturation constant for electron acceptors (mol L^{-1}).

A cybernetic modeling approach [*Song et al*., 2014] was used to account for biological regulation. The cybernetic approach views a microbial community as an optimal control strategist that selectively catalyzes alternative reaction pathway options to optimize a certain metabolic objective (e.g., total carbon uptake in this work) [*Ramkrishna and Song*, 2012]. The functional form of the enzyme levels in Eq. (4) is given as follows [*Kompala et al.*, 1986; *Young and Ramkrishna*, 2007]:

$$e_i = \frac{r_i^{kin}}{\sum_{i=1}^{3} r_i^{kin}} \quad . \tag{6}$$

Finally, the reaction rate r_i was subtracted by a fixed biomass degradation ratio k_{deg} [1/d] then multiplied by biomass concentration to calculate mass balance for each species (more details about the cybernetic model are included in the Supporting Information).

186 The cybernetic modeling formulation provides a rational description of dynamic regulation
187 without using empirical inhibitive kinetics. Literature values were used for the half-saturation
188 constants (i.e., $K_{a,i}$ and $K_{d,i}$) [*Rittmann and McCarty*, 2001; *Yan et al.*, 2016] in all reactions. The
189 energy-producing fraction parameter (f_i) and maximum specific uptake rate of microbial reaction
190 (k_i) of the two-step denitrification were obtained by fitting the model to laboratory experimental
191 data measured on HZ sediments from the site [*Li et al.*, 2017, manuscripts submitted to
192 *Envrimental Microbioglogy*]. The f_i and k_i for oxidative respiration were estimated based on
193 denitrification fitting results by assuming oxidative respiration is energetically more favorable
194 than NO_3^- reduction (reaction parameters are summarized in the Supporting Information).

195

196 We also considered the effect of temperature on reaction rate using the Arrhenius equation:

197 $$r = Ae^{\frac{-E_a}{RT}}, \quad (7)$$

198 where r is the rate constant, E_a is the activation energy (0.65 ev in this study), R is the gas
199 constant (8.314 J mol^{-1} K^{-1}), T is the temperature in Kelvin, and A is the pre-exponential factor.
200 The base reaction rates were derived from batch experiments were conducted under 26ºC. All the
201 reaction rates under other temperatures were scaled from the base rates using Eq. (7).

202 **2.3.2 Simulator and Boundary Conditions**

203 The massively parallel subsurface flow and reactive transport code PFLOTRAN [*Hammond et*
204 *al.*, 2014] was used to simulate coupled thermal-hydro-biogeochemical processes. The governing
205 flow equation in PFLTORAN is the Richards equation with Darcy's law, fully coupled to the
206 energy conservation equation for heat transport. The solute transport mechanisms include
207 advection and macrodispersion, while molecular diffusion was neglected because of its small

208 contribution compared to the macrodispersion in the presence of heterogeneity in permeability
209 field. We customized the reaction network described in Section 2.3.1 using reaction sandbox in
210 PFLOTRAN. Simulations were performed for a six-year time window (2010-2015). The first
211 year was used for model spin-up, while the other five years were used for analysis.
212
213 A transient hydrostatic hydraulic head and a Dirichlet temperature boundary condition were used
214 at both the river and inland boundaries. A seepage face was applied at the river bank exposed to
215 the atmosphere. Water level and temperature data were taken from a nearby gauge in the
216 Columbia River and the inland monitoring well, as shown in Figures 2a and 2b. The top and
217 bottom boundaries were set as no-flow and no heat transfer, as surface recharge is small in the
218 semi-arid climate zone [*Rockhold et al.*, 1995], while the bottom of the modeling domain is
219 constrained by the fine-grained Ringold formation that serves as a local aquitard.
220
221 Based on field sampling results, both the river water and groundwater are rich in dissolved
222 oxygen (~100% for river water and ~80% for groundwater). The solute boundary conditions for
223 CH_2O, HCO_3^-, and NO_3- were taken from averaged field sampling results [*Zachara et al*., 2012;
224 2016] (more information is provided in the Supporting Information). Dissolved organic carbon
225 carried by the river water was assumed to be the carbon source, i.e., CH_2O, for the
226 biogeochemical processes in the HZ, while groundwater was the source for NO_3^-. The high
227 dissolved oxygen and low dissolved organic carbon concentrations implied that aerobic
228 respiration was the dominant HZ biogeochemical process at the site [*Stegen et al.*, 2016].
229

230 **3. Results and Discussion**

231 **3.1 River Discharge and Stage Spectral Analysis Results**

232 The time-averaged wavelet power in wavelet-based spectral analysis represents the relative
233 contribution of variation at a given frequency to total variation. The higher the time-averaged
234 wavelet power, the more significant the frequency is in the entire spectrum window. Real and
235 naturalized discharges at the Priest Rapids Dam (Figure 2c) showed vastly distinct peak flows
236 and seasonal patterns over the course of a year. However, their spectral analyses (Figure 2d)
237 revealed the dominance of semi-annual and annual cycles in both time series, evident in the
238 peaks of averaged wavelet powers. Furthermore, visible peaks in wavelet powers at daily to
239 weekly frequencies were detected in observed discharge, which correspond to high-frequency
240 flow variations caused by dam operations. The sub-daily frequency, limited by the daily
241 resolution of the discharge data, was not available. The spectral analysis on the hourly river stage
242 data (Figure 2e) showed a visible peak at the daily frequency, a weak peak at the weekly
243 frequency, and two dominant peaks at the semi-annual and annual frequencies, which is
244 consistent with the discharge data and characteristic frequencies of regional electric demand.
245
246 Moving window sizes of one day and one week then were applied to the observed river stage
247 data for removing the two most important frequencies of flow variations induced by dam
248 operations. Spectral analyses applied on these two smoothed hydrographs (Figure 2e) confirmed
249 the removal of daily frequency after applying a daily smoothing window and exclusion of both
250 daily and weekly frequencies after imposing the weekly moving average. The same smoothing
251 procedure was applied to the inland groundwater table data to generate consistent hydrologic
252 boundary conditions at the both ends of model domain.
253

3.2 Effects of High-Frequency Flow Variations on Thermal Regime

Our simulations revealed a cold zone in the middle of alluvium in summer (Figure 3a), which was ~5ºC colder than the adjacent inland groundwater and river water. To better illustrate the long-term thermal dynamics in multiple depths of the HZ, we took a one-dimensional (1D) vertical slice from the 2D model domain (the black vertical line marked in Figure 3a) and generated a heat map of its temperature over time as shown in Figure 3b. This vertical slice was approximately in the center of the river stage fluctuation zone. We overlaid river stage time series and depths of the Hanford and Ringold formations on the heat map to inspect the interactions between thermal spatio-temporal dynamics and river dynamics. As evident in Figure 3b, the intrusion of cold river water in winter and early spring gradually cooled the shallow alluvium. This cold zone moved deeper into the riverbed with the intrusion flow. The temperature in shallow HZ started to increase in summer with the intrusion of warm river water. The propagation of warm zone followed a similar pattern with that of the cold zone. Although the size of this cold zone varies over the seasons, it could persist in the HZ for half a year to nearly a year as demonstrated in our simulation results. This phenomenon is consistent with field observations that discovered persistent (for months) heat storage in the HZ at our site and else where [*Arrigoni et al.*, 2008; *Burkholder et al.*, 2008]. The temperature data collected by thermistors installed at various depths below the riverbed at our site (Figure 3e) showed persisting cooler temperature at 24 cm and 64 cm depths below the riverbed, where the measured temperature was 4~5ºC lower than both the river and inland water temperatures in July. This low temperature was similar to the river water temperature in April, indicating long residence time of river water in the groundwater system [*McCallum and Shanafield*, 2016] and/or heat storage effect of the aquifer sediments [*Constantz*, 2008].

The persistence of cold zone was also yielded in the simulations driven by daily and weekly smoothed boundaries. The differences in temperature fields between the base case and daily and weekly smoothed cases represent the effects of high-frequency flow variations on the HZ thermal regime. There was negligible difference between the daily and weekly smoothed cases, indicating most of differences were caused by daily to sub-daily variations. We only included the differences between the base case and weekly smoothed case (Figure 3c) for brevity. Under the high-frequency river fluctuation, the shallow HZ became ~10ºC colder in winter and early spring (the blue areas in Figure 3c) and ~5ºC warmer in summer and early fall (the red areas in Figure 3c), meaning the heat exchange between river water and HZ was enhanced. The maximum difference in Figure 3c was capped at 5ºC to show fine details of temperature difference. It was also demonstrated in Figures 3c and 3d that more significant temperature differences were resulted when the low river stage was low, usually between fall and early winter. The high-frequency flow variations had little effect on hyporheic exchange flow during high river stage because they could hardly change the dominant inflow direction. However, the high-frequency fluctuations could induce more frequent changes in flow directions at low river stage. Thus, enhancing the exchange of mass and heat between the river and groundwater systems. The high-frequency flow variations enhanced the intrusion of cool river water in winter to yield cooler HZ, while they led to warmer HZ temperature during summer time. Significantly warmer HZ temperature was resulted in the summer and fall of 2015 due to an extreme drought conditions caused by thin snowpack in the headwater catchments.

299 As the benthic temperature impacts fish spawning and growth [*Mejia et al.*, 2016], the stronger
300 impact of high-frequency flow variations on the HZ thermal regime under low flow conditions
301 has significant ecological implications with respect to dam operations. For example, dam
302 operations in winter could cool down sediments and store cold water to buffer the temperature
303 increase in summer, creating thermal refugia for coldwater fishes [*Caissie*, 2006; *Kurylyk et al.*,
304 2015; *Whitledge et al.*, 2006]. However, dam operations during drought years should be planned
305 to minimize potential adverse ecological consequences.

306

307 **3.3 Effects of High-Frequency Flow Variations on Biogeochemical Reactions**

308 Cumulative carbon consumption was quantified in each grid cell for baseline and smoothed cases
309 to identify the hot spots of biogeochemical reactions and assess the potential impacts of high-
310 frequency flow variations. Our key observations included: 1) The alluvial layer was the most
311 biogeochemically active domain as reflected by the total carbon consumption shown in Figure 4a,
312 which was consistent with the results obtained by *Gu et al.* [2012] assuming homogenous
313 permeability; and 2) the spatial distribution of biogeochemically active zones was similar to that
314 of the mean velocity field during the simulation window (Figure 4b), indicating the dependence
315 of biogeochemical processes on flow and transport processes. The scatter plots between
316 cumulative carbon consumption and velocity (Figure 4d) and between cumulative carbon
317 consumption and permeability (Figure 4e) confirmed the strong dependence of total carbon
318 consumption on hydrogeologic properties of HZ, which consequently controls the flow paths that
319 influence residence times and nutrient supply. Most of the carbon was consumed by oxidative
320 respiration (89.24% out of total consumption) because both the groundwater and river water
321 were well oxygenated.

The weekly smoothed case (Figure 4c) yielded very similar spatial pattern of total carbon consumption compared to the baseline case, implying similar intrusion paths under smoothed boundary conditions. Thus, high-frequency flows had negligible influence on the locations of biogeochemical hotspots under the assumption of river water being the only carbon source. However, more carbon consumption within the Hanford formation was observed in Figure 4a than in Figure 4c, due to the enhanced hyporheic exchange. Similar to the impact on the thermal regime, the high-frequency flow variations had stronger impact on total carbon consumption during low river stage (Figure 4f) by transporting more organic carbon from the river into the HZ through enhanced exchange flows. The enhanced hyporheic biogeochemical processes driven by the high-frequency flow variations could have attendant effects on riverine benthic food webs [*Baxter et al.*, 2005; *Richardson et al.*, 2010], fish spawning [*Mejia et al.*, 2016], and organic contaminant biodegradation [*Conant et al.*, 2004]. These biogeochemical effects may be compounded at the low river stage when HZ temperature also is highly impacted by high-frequency flow variations.

4. Conclusion

High-frequency flow variations are a common phenomenon in most regulated river systems, which experience more abrupt and frequent fluctuations than in natural rivers. It has been previously reported that river regulation by dam operation can enhance hydrologic exchange within and through the HZ, but the attendant effects on the long-term thermal regime and biogeochemical processes of the HZ have not been established. We provided an initial assessment of these significant effects in this communication using a newly developed thermal-hydro-biogeochemical model, lab-calibrated reaction rates for key biogeochemical reactions, and field monitoring data. Our results showed that the high-frequency flow variations enhanced

hyporheic exchange, increased biogeochemical fluxes, and created long-term alterations to thermal regimes. The impact of high-frequency flow variations was maximized during drought conditions (low river stage periods) by creating more frequent changes in exchange flow directions. However, the spatial distribution of biogeochemical hot spots was less influenced by flow variation while highly dependent on subsurface hydraulic properties.

The temperature and biogeochemical dynamics in the HZ are important to fluvial ecology, such as thermal refugia for fish spawning and growth, benthic food production, and nitrate removal. As a regulated system, the Hanford Reach of the Columbia River is not unusual in experiencing strong daily and weekly rhythms driven by hydropower demands that shift the thermal and biogeochemical regimes in the HZ. This study provided the scientific basis to assess the potential ecological consequences of the high-frequency flow variations in a regulated river, as well as guidance on how to maximize the potential benefits—or minimize the drawbacks—of river regulation to river ecosystems.

Acknowledgments

This research was supported by the U.S. Department of Energy (DOE), Office of Biological and Environmental Research (BER), as part of BER's Subsurface Biogeochemistry Research Program (SBR). This contribution originates from the SBR Scientific Focus Area (SFA) at Pacific Northwest National Laboratory (PNNL). This research used resources of the National Energy Research Scientific Computing Center, a DOE Office of Science User Facility supported by the DOE's Office of Science under Contract No. DE-AC02-05CH11231. Requests for data

not explicitly provided in the manuscript may be made to the corresponding author. PNNL is operated by Battelle for the DOE under Contract DE-AC05-76RL01830.

References

Arntzen, E. V., D. R. Geist, and P. E. Dresel (2006), Effects of fluctuating river flow on groundwater/surface water mixing in the hyporheic zone of a regulated, large cobble bed river, *River Res. Appl.*, **22**(8), 937-946.

Arrigoni, A. S., G. C. Poole, L. A. K. Mertes, S. J. O'Daniel, W. W. Woessner, and S. A. Thomas (2008), Buffered, lagged, or cooled? Disentangling hyporheic influences on temperature cycles in stream channels, *Water Resour. Res.*, **44**(9), W09418.

Battin, T. J., L. A. Kaplan, S. Findlay, C. S. Hopkinson, E. Marti, A. I. Packman, J. D. Newbold, and F. Sabater (2008), Biophysical controls on organic carbon fluxes in fluvial networks, *Nat. Geosci.*, **1**(2), 95-100.

Baxter, C. V., K. D. Fausch, and W. Carl Saunders (2005), Tangled webs: Reciprocal flows of invertebrate prey link streams and riparian zones, *Freshwater Biol.*, **50**(2), 201-220.

Bjornstad, B., D. Lanigan, J. Horner, P. Thorne, and V. Vermeul (2009), Borehole completion and conceptual hydrogeologic model for the IFRC well field, 300 Area, Hanford Site*, Rep. PNNL-18340*, Pacific Northwest National Laboratory (PNNL), Richland, WA (US).

Boano, F., J. W. Harvey, A. Marion, A. I. Packman, R. Revelli, L. Ridolfi, and A. Wörman (2014), Hyporheic flow and transport processes: Mechanisms, models, and biogeochemical implications, *Rev. Geophys.*, **52**(4), 603-679.

Boulton, A. J., S. Findlay, P. Marmonier, E. H. Stanley, and H. M. Valett (1998), The functional significance of the hyporheic zone in streams and rivers, *Annu. Rev. Ecol. Syst.*, **29**(1), 59-81.

Briody, A. C., M. B. Cardenas, P. Shuai, P. S. K. Knappett, and P. C. Bennett (2016), Groundwater flow, nutrient, and stable isotope dynamics in the parafluvial-hyporheic zone of the regulated Lower Colorado River (Texas, USA) over the course of a small flood, *Hydrogeol. J.*, **24**(4), 923-935.

Brunke, M., and T. O. M. Gonser (1997), The ecological significance of exchange processes between rivers and groundwater, *Freshwater Biol.*, **37**(1), 1-33.

Buffington, J. M., and D. Tonina (2009), Hyporheic exchange in mountain rivers II: Effects of channel morphology on mechanics, scales, and rates of exchange, *Geography Compass.*, **3**(3), 1038-1062.

Burkholder, B. K., G. E. Grant, R. Haggerty, T. Khangaonkar, and P. J. Wampler (2008), Influence of hyporheic flow and geomorphology on temperature of a large, gravel-bed river, Clackamas River, Oregon, USA, *Hydrol. Processes*, **22**(7), 941-953.

Caissie, D. (2006), The thermal regime of rivers: A review, *Freshwater Biol.*, **51**(8), 1389-1406.

Cardenas, M. B. (2015), Hyporheic zone hydrologic science: A historical account of its emergence and a prospectus, *Water Resour. Res.*, **51**(5), 3601-3616.

Cardenas, M. B., and J. L. Wilson (2007), Dunes, turbulent eddies, and interfacial exchange with permeable sediments, *Water Resour. Res.*, **43**(8), W08412.

Cardenas, M. B., J. L. Wilson, and V. A. Zlotnik (2004), Impact of heterogeneity, bed forms, and stream curvature on subchannel hyporheic exchange, *Water Resour. Res.*, **40**(8), W08307.

Casas-Mulet, R., K. Alfredsen, Å. Brabrand, and S. J. Saltveit (2016), Hydropower operations in groundwater-influenced rivers: Implications for Atlantic salmon, Salmo salar, early life stage development and survival, *Fisheries Manag. Ecol.*, **23**(2), 144-151.

Chen, X., G. E. Hammond, C. J. Murray, M. L. Rockhold, V. R. Vermeu, and J. M. Zachara (2013), Application of ensemble-based data assimilation techniques for aquifer characterization using tracer data at Hanford 300 area, *Water Resour. Res.*, **49**(10), 7064-7076.

Conant, B., J. A. Cherry, and R. W. Gillham (2004), A PCE groundwater plume discharging to a river: Influence of the streambed and near-river zone on contaminant distributions*, J. Contam. Hydrol.*, **73**(1), 249-279.

Constantz, J. (2008), Heat as a tracer to determine streambed water exchanges, *Water Resour. Res.*, **44**(4), W00D10.

Duncan, J. P., K. W. Burk, M. A. Chamness, R. A. Fowler, B. G. Fritz, P. L. Hendrickson, E. P. Kennedy, G. V. Last, T. M. Poston, and M. R. Sackschewsky (2007), Hanford Site National Environmental Policy Act (NEPA) characterization, *Rep.PNNL-6415 Rev.18*, Pacific Northwest National Laboratory (PNNL), Richland, WA (US).

Ebersole, J. L., W. J. Liss, and C. A. Frissell (2003), Thermal heterogeneity, stream channel morphology, and salmonid abundance in northeastern Oregon streams*, Can. J. Fish. Aquat. Sci.*, **60**(10), 1266-1280.

Francis, B. A., L. K. Francis, and M. B. Cardenas (2010), Water table dynamics and groundwater-surface water interaction during filling and draining of a large fluvial island due to dam-induced river stage fluctuations, *Water Resour. Res.*, **46**(7), W07513.

Fritz, B. G., and E. V. Arntzen (2007), Effect of rapidly changing river stage on uranium flux through the hyporheic zone, *Ground Water*, **45**(6), 753-760.

Galbraith, H. S., C. J. Blakeslee, and W. A. Lellis (2012), Recent thermal history influences thermal tolerance in freshwater mussel species (Bivalvia: Unionoida), *Freshw. Sci.*, **31**(1), 83-92.

Geist, D. R., T. P. Hanrahan, E. V. Arntzen, G. A. McMichael, C. J. Murray, and Y.-J. Chien (2002), Physicochemical characteristics of the hyporheic zone affect redd site selection by chum salmon and fall chinook salmon in the Columbia River, *N. Am. J. Fish. Manage.*, **22**(4), 1077-1085.

Gerecht, K. E., M. B. Cardenas, A. J. Guswa, A. H. Sawyer, J. D. Nowinski, and T. E. Swanson (2011), Dynamics of hyporheic flow and heat transport across a bed-to-bank continuum in a large regulated river, *Water Resour. Res.*, **47**(3), W03524.

Graf, W. L. (1999), Dam nation: A geographic census of American dams and their large-scale hydrologic impacts, *Water Resour. Res.*, **35**(4), 1305-1311.

Graham, P. W., M. S. Andersen, M. F. McCabe, H. Ajami, A. Baker, and I. Acworth (2015), To what extent do long-duration high-volume dam releases influence river–aquifer interactions? A case study in New South Wales, Australia, *Hydrogeol. J.*, **23**(2), 319-334.

Gu, C., W. Anderson, and F. Maggi (2012), Riparian biogeochemical hot moments induced by stream fluctuations, *Water Resour. Res.*, **48**(9), W09546.

Hammond, G. E., P. C. Lichtner, and R. T. Mills (2014), Evaluating the performance of parallel subsurface simulators: An illustrative example with PFLOTRAN, *Water Resour. Res*, **50**(1), 208-228.

Hanrahan, T. P. (2007), Large-scale spatial variability of riverbed temperature gradients in Snake River fall Chinook salmon spawning areas, *River Res. Appl.*, **23**(3), 323-341.

Kompala, D. S., D. Ramkrishna, N. B. Jansen, and G. T. Tsao (1986), Investigation of bacterial growth on mixed substrates: Experimental evaluation of cybernetic models, *Biotechnol. Bioeng.*, **28**(7), 1044-1055.

Kurylyk, B. L., K. T. MacQuarrie, T. Linnansaari, R. A. Cunjak, and R. A. Curry (2015), Preserving, augmenting, and creating cold-water thermal refugia in rivers: Concepts derived from research on the Miramichi River, New Brunswick (Canada), *Ecohydrol.*, **8**(6), 1095-1108.

Lautz, L. K., and R. M. Fanelli (2008), Seasonal biogeochemical hotspots in the streambed around restoration structures, *Biogeochemistry*, **91**(1), 85-104.

Ma, R., C. Zheng, J. M. Zachara, and M. Tonkin (2012), Utility of bromide and heat tracers for aquifer characterization affected by highly transient flow conditions, *Water Resour. Res.*, **48**, W08523.

McCallum, J. L., and M. Shanafield (2016), Residence times of stream-groundwater exchanges due to transient stream stage fluctuations, *Water Resour. Res.*, **52**(3), 2059-2073.

McClain, M. E., E. W. Boyer, C. L. Dent, S. E. Gergel, N. B. Grimm, P. M. Groffman, S. C. Hart, J. W. Harvey, C. A. Johnston, E. Mayorga, W. H. McDowell, and G. Pinay (2003), Biogeochemical hot spots and hot moments at the interface of terrestrial and aquatic ecosystems, *Ecosystems*, **6**(4), 301-312.

Mejia, F. H., C. V. Baxter, E. K. Berntsen, and A. K. Fremier (2016), Linking groundwater – surface water exchange to food production and salmonid growth1, *Can. J. Fish. Aquat. Sci.*, **73**(11), 1650-1660.

Nilsson, C., C. A. Reidy, M. Dynesius, and C. Revenga (2005), Fragmentation and flow regulation of the world's large river systems, *Science*, **308**(5720), 405-408.

475 Pebesma, E. J. (2004), Multivariable geostatistics in S: the gstat package, *Comput. Geosci.*, **30**(7),
476 683-691.

477 Ramkrishna, D., and H.-S. Song (2012), Dynamic models of metabolism: Review of the
478 cybernetic approach, *AIChE J.*, **58**(4), 986-997.

479 Richardson, J. S., Y. Zhang, and L. B. Marczak (2010), Resource subsidies across the land–
480 freshwater interface and responses in recipient communities, *River Res. Appl.*, **26**(1), 55-66.

481 Rittmann, B. E., and P. L. McCarty (2001), *Environmental Biotechnology*: *Principles and*
482 *Applications*, 768 pp., McGraw-Hill, New York City, NY.

483 Rockhold, M. L., M. J. Fayer, C. T. Kincaid, and G. W. Gee (1995), Estimation of natural
484 groundwater recharge for the performance assessment of a low-level waste disposal facility at
485 the Hanford Site*, Rep. PNL-10508*, Pacific Northwest National Laboratory, Richland, WA (US).

486 Roesch, A., and H. Schmidbauer (2015), WaveletComp: Computational wavelet analysis, R
487 Package Version, 1.0. https://cran.r-project.org/web/packages/WaveletComp/WaveletComp.pdf.

488 Salehin, M., A. I. Packman, and M. Paradis (2004), Hyporheic exchange with heterogeneous
489 streambeds: Laboratory experiments and modeling, *Water Resour. Res.*, **40**(11), W11504.

490 Schmadel, N. M., A. S. Ward, C. S. Lowry, and J. M. Malzone (2016), Hyporheic exchange
491 controlled by dynamic hydrologic boundary conditions, *Geophys. Res. Lett.*, **43**(9), 4408-4417.

492 Slater, L. D., D. Ntarlagiannis, F. D. Day-Lewis, K. Mwakanyamale, R. J. Versteeg, A. Ward, C.
493 Strickland, C. D. Johnson, and J. W. Lane (2010), Use of electrical imaging and distributed
494 temperature sensing methods to characterize surface water-groundwater exchange regulating
495 uranium transport at the Hanford 300 Area, Washington, *Water Resour. Res.*, **46**(10), W00153.

496 Song, H. S., W. R. Cannon, A. S. Beliaev, and A. Konopka (2014), Mathematical modeling of
497 microbial community dynamics: A methodological review, *Processes*, 2(4), 711-752.

498 Stegen, J. C., J. K. Fredrickson, M. J. Wilkins, A. E. Konopka, W. C. Nelson, E. V. Arntzen, W.
499 B. Chrisler, R. K. Chu, R. E. Danczak, S. J. Fansler, D. W. Kennedy, C. T. Resch, and M. Tfaily
500 (2016), Groundwater-surface water mixing shifts ecological assembly processes and stimulates
501 organic carbon turnover, *Nat. Commun.*, **7**, 11237.

502 Stonedahl, S. H., J. W. Harvey, and A. I. Packman (2013), Interactions between hyporheic flow
503 produced by stream meanders, bars, and dunes, *Water Resour. Res.*, **49**(9), 5450-5461.

504 Sawyer, A. H., M. B. Cardenas, A. Bomar, and M. Mackey (2009), Impact of dam operations on
505 hyporheic exchange in the riparian zone of a regulated river, *Hydrol. Processes*, **23**(15), 2129-
506 2137.

507 Trauth, N., and J. H. Fleckenstein (2017), Single discharge events increase reactive efficiency of
508 the hyporheic zone, *Water Resour. Res.*, accepted, DOI: 10.1002/2016WR019488.

509 Vogt, T., M. Schirmer, and O. Cirpka (2012), Investigating riparian groundwater flow close to a
510 losing river using diurnal temperature oscillations at high vertical resolution, *Hydrol. Earth Syst.*
511 *Sci.*, **16**(2), 473-487.

Whitledge, G. W., C. F. Rabeni, G. Annis, and S. P. Sowa (2006), Riparian shading and groundwater enhance growth potential for smallmouth bass in Ozark streams, *Ecol. Appl.*, **16**(4), 1461-1473.

Williams, M., P. Thorne, M. Rockhold, and Y. Chen (2008), Three-dimensional groundwater models of the 300 Area at the Hanford Site , Washington State*, Rep. PNNL-17708*, Pacific Northwest National Laboratory, Richland, WA (US).

Yan, S., et al. (2016), Nitrate bioreduction in redox-variable low permeability sediments, *Sci. Total Environ.*, **539**, 185-195.

Ye, S., T. P. Covino, M. Sivapalan, N. B. Basu, H. Y. Li, and S. W. Wang (2012), Dissolved nutrient retention dynamics in river networks: A modeling investigation of transient flows and scale effects, *Water Resour. Res.*, **48**(6).

Yellen, B., and D. F. Boutt (2015), Hydropeaking induces losses from a river reach: Observations at multiple spatial scales, *Hydrol. Processes*, **29**(15), 3261-3275.

Young, J. D., and D. Ramkrishna (2007), On the matching and proportional laws of cybernetic models, *Biotechnol. Prog.*, **23**(1), 83-99.

Zachara, J. M., X. Y. Chen, C. Murray, and G. Hammond (2016), River stage influences on uranium transport in a hydrologically dynamic groundwater-surface water transition zone, *Water Resour. Res.*, **52**(3), 1568-1590.

Zachara, J. M., M. D. Freshley, G. V. Last, R. E. Peterson, and B. N. Bjornstad (2012), Updated conceptual model for the 300 Area uranium groundwater plume, *Rep. PNNL-22048*, Pacific Northwest National Laboratory (PNNL), Richland, WA (US).

Zarnetske, J. P., R. Haggerty, S. M. Wondzell, and M. A. Baker (2011), Dynamics of nitrate production and removal as a function of residence time in the hyporheic zone, *J. Geophys. Res.*, **116**(G1), G01025.

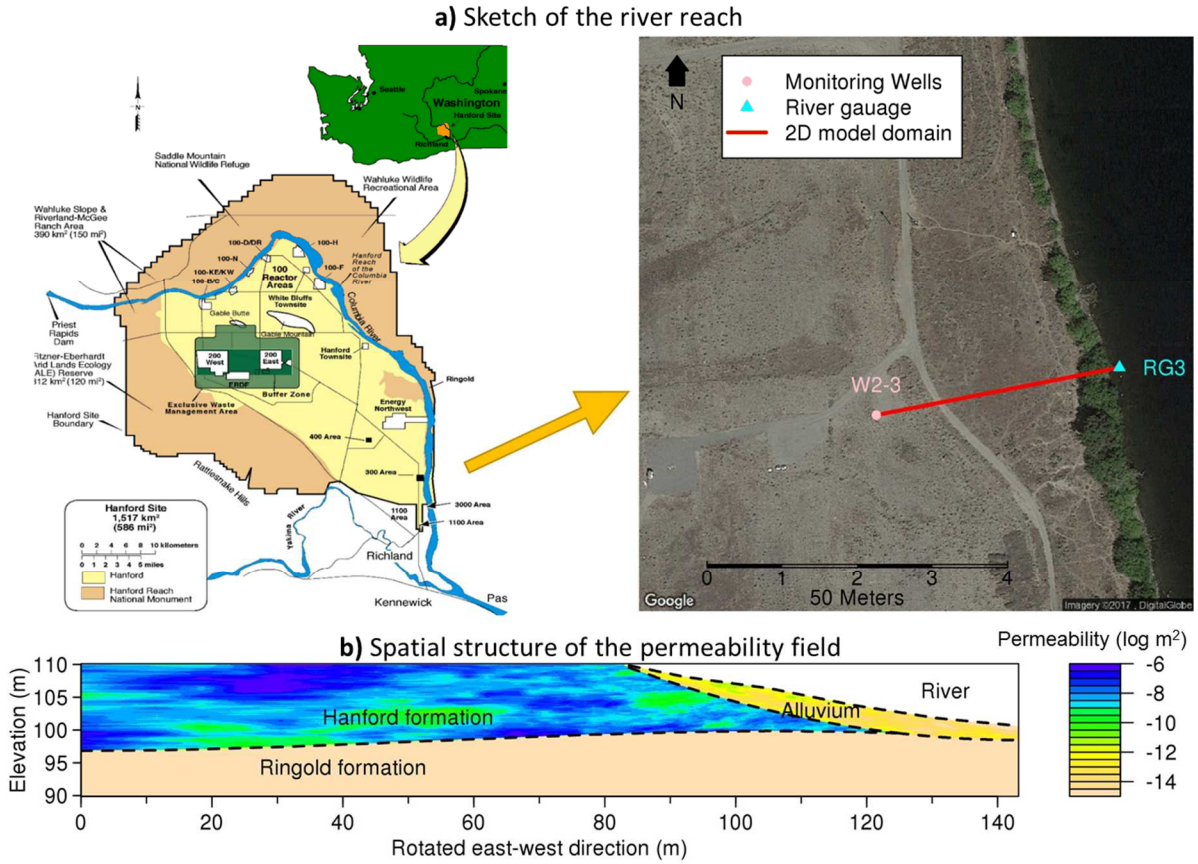

Figure 1. Location map and conceptual model: a) Sketch of the river reach. W2-3 represents the inland monitoring wells, and RG3 represents the river gauge with contiunous level and temperature data. b) Spatial structure of the permeability field.

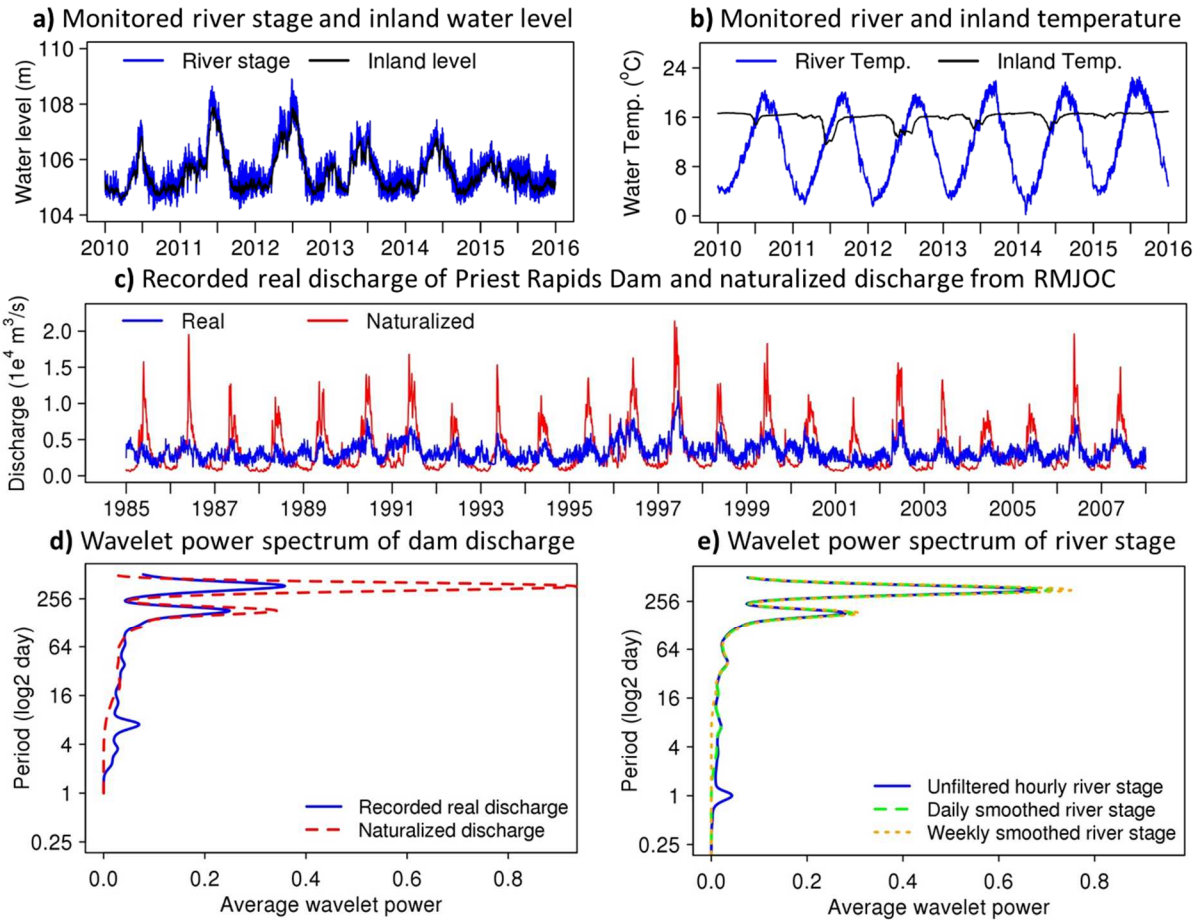

Figure 2. Monitoring data and spectral analysis results: a) Monitored river stage and inland water level; b) Monitored river and inland temperature; c) Recorded real discharge of Priest Rapids Dam and naturalized discharge from RMJOC; d) Average wavelet power spectrum of recorded real discharge and naturalized discharge from RMJOC. Higher average wavelet power on particular frequency (period) means it is more significant in the time series variation; e) Average wavelet power spectrum of unfiltered hourly river stage, daily smoothed river stage, and weekly smoothed river stage.

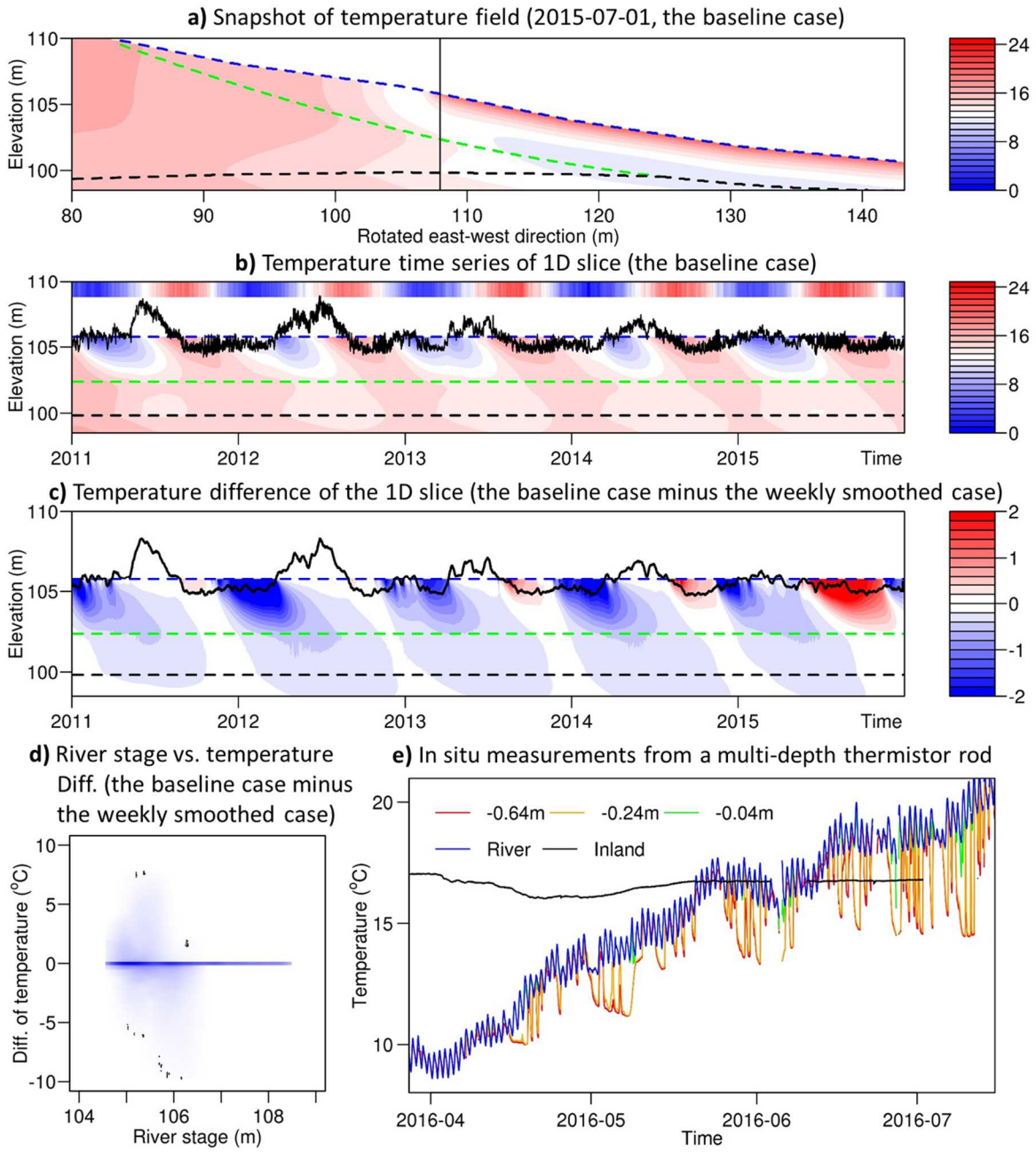

Figure 3. Temperature results: a) Snapshot of the temperature field (the baseline case), focusing on the alluvium and near-shore Hanford. The colored dash lines are the formation boundaries, and the time was taken on 07/01/2015 to illustrate the cold water zone in summer; b) Temperature time series of a 1D slice (the vertical line in 3a) of base case illustrates the temperature lags in the HZ. The top crossband shows the temperature of river water, the black curve is the river stage, the colored dash lines are the formation boundaries, and the bottom part is the temperature dynamics in this column; c) Temperature difference of the 1D slice between cases (the baseline case minus the weekly smoothed case); d) River stage versus temperature difference between cases (the baseline case minus the weekly smoothed case) in entire alluvium; f) Temperature observation from a thermistor rod. The negative labels mean those thermistors were below the river bed.

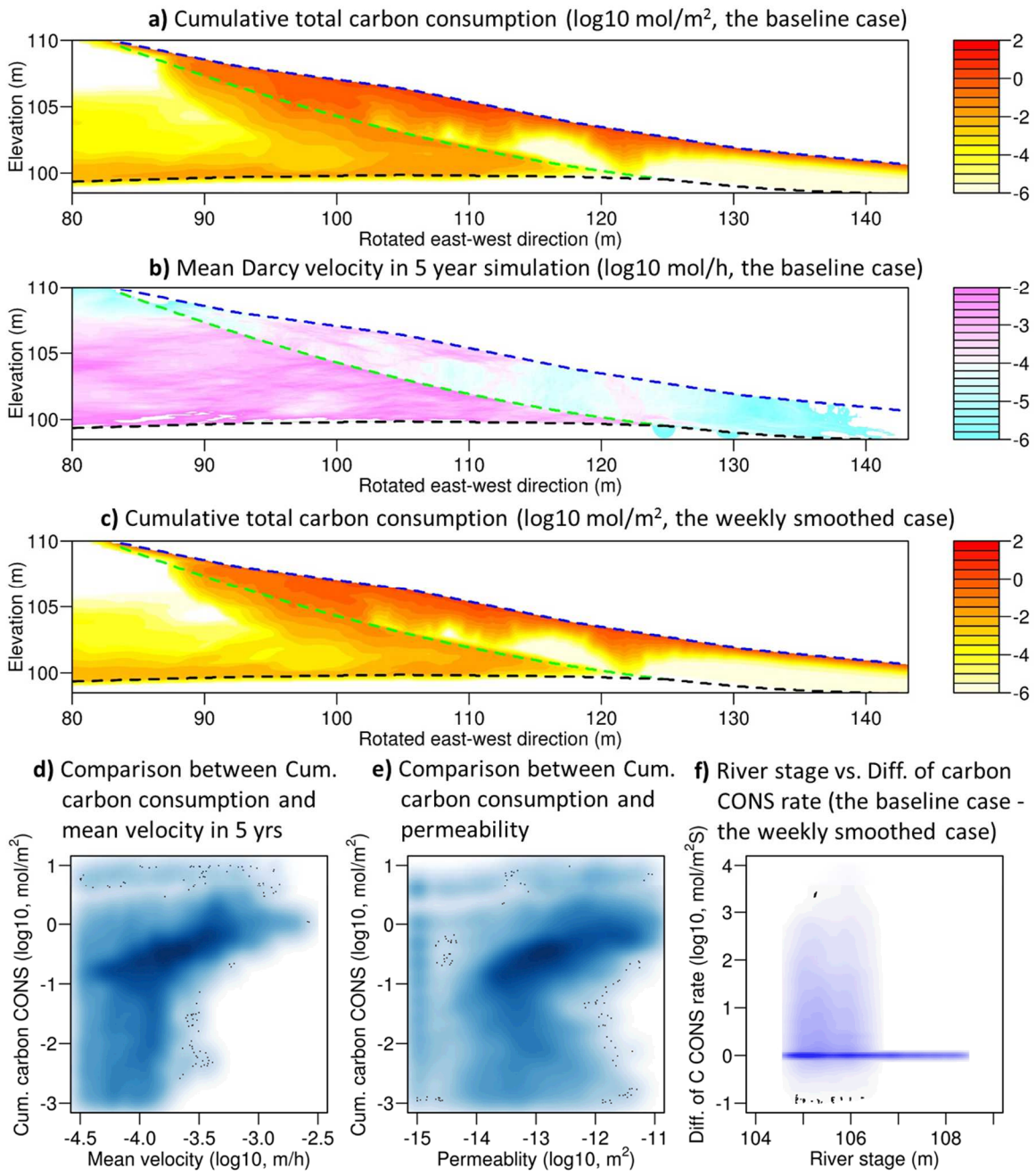

Figure 4. Biogeochemical results: a) Cumulative total carbon consumption (log10, mol/m^2) in the baseline case. The colored dash lines are the formation boundaries; b) Mean Darcy velocity field during five-year simulation (log10 m/h) in the baseline case. The colored dash lines are the formation boundaries; c) Cumulative total carbon consumption (log10, mol/m^2) in the weekly smoothed case. The colored dash lines are the formation boundaries; d) One-to-one comparsion between cumulative carbon consumption and mean velocity across the entire alluvium; e) One-to-one comparsion between cumulative carbon consumption and permeability across the entire alluvium; f) River stage versus carbon consumption rate difference between cases (the baseline case minus the weekly smoothed case) in the entire alluvium.